Z. Phys. C – Particles and Fields 38, 371–382 (1988)

Zeitschrift für Physik C Particles and Fields

Production of high transverse momentum prompt photons and neutral pions in proton-proton interactions at 280 GeV/c

WA 70 Collaboration

M. Bonesini[4], E. Bonvin[5], P.S.L. Booth[3], L.J. Carroll[3], A.J. Cass[3], D. Cavalli[4], G. Cecchet[4], G. Costa[4], M. Donnat[1], P.A. Dorsaz[1], D.N. Edwards[3], J.R. Fischer[1], L. Fluri[5], D. Frame[2], F. Gianotti[4], S. Jack[2], J.N. Jackson[3], M. Kelly[3], M.N. Kienzle-Focacci[1], R. Lucock[2], J.G. Lynch[2], L. Mandelli[4], M. Martin[1], L. Mathys[1], A. Maxwell[2], M. Mazzanti[4], J.J. Myerscough[3], P.J. Negus[2], S. Pensotti-Rancoita[4], L. Perini[4,6], D. Perrin[5], G. Polesello[4], W.H. Range[3], L. Rosselet[1], S.W. Snow[3], A.S. Thompson[2], R.M. Turnbull[2], J. Wells[2], M. Werlen[1]

[1] University of Geneva, D.P.N.C., CH-1211 Geneve, Switzerland
[2] Department of Physics and Astronomy, University of Glasgow, Glasgow, G12, 8QQ, UK
[3] Department of Physics, University of Liverpool, Liverpool, L69, 3BX, UK
[4] Dipartimento di Fiscia dell'Università e Sezione INFN Milano, I-20133 Milano, Italy
[5] University of Neuchâtel, CH-2000 Neuchâtel, Switzerland
[6] CERN, CH-1211 Geneve 23, Switzerland

Received 23 November 1987

Abstract. The inclusive cross sections for production of prompt photons and $\pi^0 s$ by 280 GeV/c protons incident on a liquid hydrogen target, have been measured for p_T in the range 4.0 to 6.5 GeV/c and for $|x_F|<0.45$. A quantitative comparison of the prompt photon cross section with next-to-leading order QCD predictions using Duke and Owens structure functions is performed. Phenomenological fits to the π^0 and prompt photon cross sections are given.

1 Introduction

A study of high transverse momentum (p_T) prompt photon production provides a clean theoretical check of the constituent dynamics in hadronic collisions [1]. In proton-proton interactions, the dominant lowest order subprocess is expected to be the "Compton scattering" process $gq \to \gamma q$, as the annihilation channel $q\bar{q} \to \gamma g$ involves only antiquarks from the sea. The prompt photon cross section together with QCD next-to-leading order calculations [2] therefore provides information on the gluon structure function for the proton. However, efficient detection of $\pi^0 s$ and ηs is necessary because these particles constitute the main source of background in the prompt photon sample.

Several experiments have investigated these processes [3–10]. The WA 70 collaboration has accumulated data from two experimental runs in 1984 and 1985, at the CERN SPS with 280 GeV/c positive and negative beams on a hydrogen target. The data presented here on the production of γ and π^0 in proton-proton interactions correspond to a sensitivity of 5.2 pb^{-1} and cover the kinematical range $4.0 < p_T < 6.5$ GeV/c and $|x_F|<0.45 (x_F \equiv 2p_{\parallel \text{cm}}/\sqrt{s})$. Results from this experiment on the production of γs and $\pi^0 s$ in $\pi^- p$ and $\pi^+ p$ interactions are presented elsewhere [11, 12].

The experimental system is briefly presented in Sec. 2. In Sec. 3 the analysis procedures common to $\pi^0 s$ and prompt photons are described. The selection criteria, efficiencies and results are given for the $\pi^0 s$ in Sec. 4 and for prompt photons in Sec. 5. A quantitative comparison of the prompt photon data with next-to-leading order QCD predictions is given in Sec. 6, followed by conclusions in Sec. 7.

2 The experimental system

The experiment, described in more detail elsewhere [12], was carried out at the CERN SPS, using a 280 GeV/c unseparated hadron beam incident on a 1 m long hydrogen target. Two differential 'CEDAR'

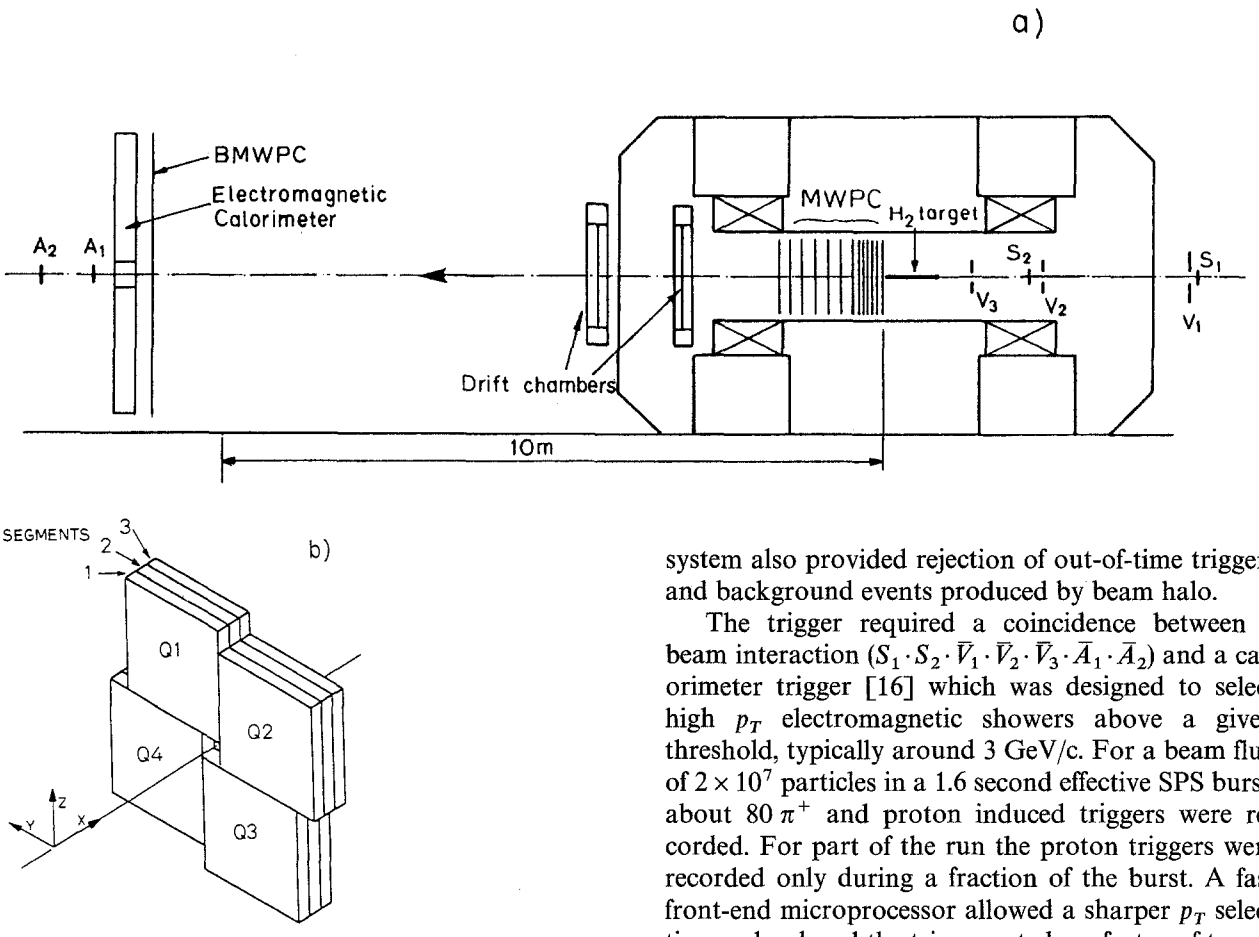

Fig. 1a, b. The experimental system. **a** The experimental layout (in 1984 only one drift chamber was used). **b** The electromagnetic calorimeter

Cerenkov counters [13], each with eight photomultipliers, were tuned to identify positive pions. A beam particle giving signals in less than three of the sixteen photomultipliers was defined as a proton (69% of the beam particles). A lead-liquid scintillator electromagnetic calorimeter [14] and a multiwire proportional chamber (BMWPC), with fiducial areas of 4 m × 4 m, were used together with the Omega spectrometer (Fig. 1a).

The calorimeter (Fig. 1b), placed 10.9 m from the downstream end of the target, consists of twelve segments arranged in quadrants, each three segments deep with orthogonal readout. A segment contains ten sheets of lead (4.2 mm thick), interleaved with ten layers of teflon tubes (4.4 mm diameter) filled with liquid scintillator, giving a total of 24 radiation lengths for each quadrant. A time-of-flight (TOF) electronics system [15] in the upstream segment of the calorimeter was used to resolve spatial ambiguities in multishower events by measuring the transit time of the scintillator light along the teflon tubes. This system also provided rejection of out-of-time triggers and background events produced by beam halo.

The trigger required a coincidence between a beam interaction ($S_1 \cdot S_2 \cdot \bar{V}_1 \cdot \bar{V}_2 \cdot \bar{V}_3 \cdot \bar{A}_1 \cdot \bar{A}_2$) and a calorimeter trigger [16] which was designed to select high p_T electromagnetic showers above a given threshold, typically around 3 GeV/c. For a beam flux of 2×10^7 particles in a 1.6 second effective SPS burst, about 80 π^+ and proton induced triggers were recorded. For part of the run the proton triggers were recorded only during a fraction of the burst. A fast front-end microprocessor allowed a sharper p_T selection and reduced the trigger rate by a factor of two.

Decaying pions produce an extended halo of muons around the beam line, leading to showers in the calorimeter from bremsstrahlung radiation. These showers can appear to have a large p_T and produce a trigger in random coincidence with an otherwise low p_T interaction. In 1985, these false triggers from muon halo were reduced by adding a toroidal magnet which surrounded the beam line 80 m upstream of the target. In addition, a set of ten scintillation counters was installed upstream of the hydrogen target, covering the median region of the calorimeter, to tag these triggers.

3 Data reduction

The calorimeter pattern recognition program [14] reconstructs the showers by matching the amplitude information from the two orthogonal coordinates in each quadrant, as well as the TOF information and the longitudinal development of the showers. From this information, different hypotheses of shower configurations within a quadrant have been constructed for each event. Only the more probable hypotheses have been considered and classified by taking into account the non-associated energy and the global χ^2

formed by energy, longitudinal shower development and TOF information. For 75% of the events, more than one hypothesis were acceptable, but the trigger shower was unambiguously selected in 95% of the events. For the π^0 analysis, only the best hypothesis has been used, while for the prompt photon selection all hypotheses have been considered in the trigger quadrant in order to provide a stronger rejection against $\pi^0 s$ and ηs.

The length of the ADC gate (110 ns) and the high beam intensity could lead to events where the showers in the calorimeter were produced by more than one beam-target interaction. The TOF information was used to reject interactions separated by more than 7.5 ns.

Charged tracks and interaction vertices have been reconstructed by TRIDENT, the standard Omega pattern recognition program.

Events with a trigger shower, defined as the highest p_T shower in the trigger quadrant, have been selected by the following criteria [12]:

a) The reconstructed vertex is inside the volume of the target.

b) For rejection of superposed events, the TOF information of the full event is consistent with a single interaction inside the target.

c) For rejection of muon halo triggers, the TOF of the trigger shower is within 1.2 ns of other showers in the event, the trigger shower points to the target and there is no corresponding signal in the muon halo veto counters (1985 only) and in the BMWPC.

d) For rejection of charged and neutral hadronic showers, the energy deposited in the third segment is less than 20% of the total energy of the shower and there is a TOF signal for the trigger shower.

e) For rejection of charged particles, including electrons, no track in the Omega MWPCs extrapolates to within 5 cm of the trigger shower and there is no corresponding signal in the BMWPC.

4 π^0 analysis and results

4.1 *Identification*

For the π^0 analysis, the trigger shower from the best hypothesis has been combined with all other showers to form $\gamma\gamma$ effective masses. In order to minimize the combinatorial background, only those combinations with the decay asymmetry $|E_{\gamma_1}-E_{\gamma_2}|/(E_{\gamma_1}+E_{\gamma_2})$ less than 0.9 have been accepted.

The resulting $\gamma\gamma$ mass spectrum is shown in Fig. 2; it is seen that the π^0 mass resolution (σ) is 10 MeV. Candidates for π^0 events have been selected with the $\gamma\gamma$ effective mass in the range 85 to 185 MeV. The background under the π^0 peak, evaluated by fitting

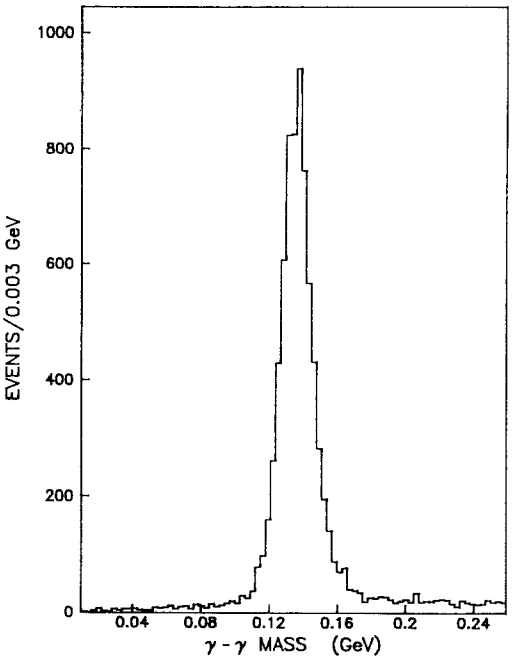

Fig. 2. The $\gamma\gamma$ effective mass spectrum in the π^0 mass region

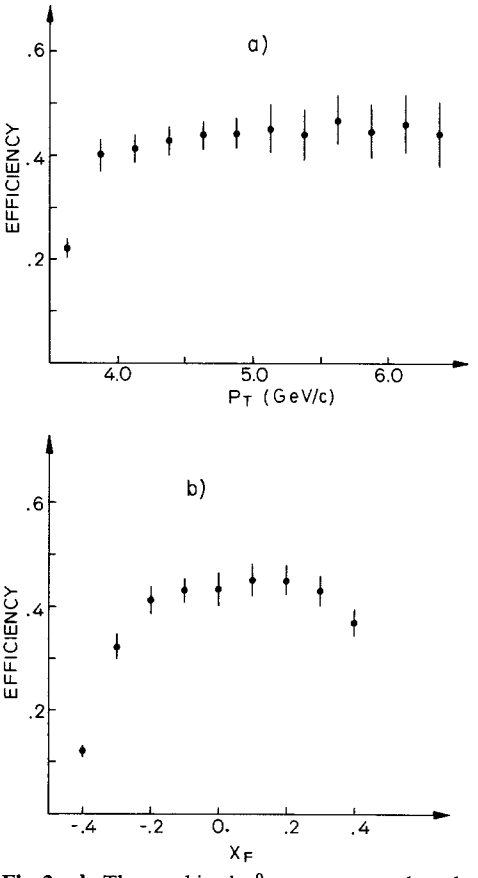

Fig. 3a, b. The combined π^0 acceptance and analysis efficiency, as obtained by Monte Carlo and by analysis of rejected events. **a** $|x_F|$ <0.15. Only the region $p_T>4.0$ GeV/c has been used. **b** $4.5<p_T$ <5.0 GeV/c. The error bars include the Monte Carlo statistical errors and systematic uncertainties as well as the estimated systematic effects from rejected events. The errors are added in quadrature

the mass spectrum with a gaussian and a polynomial function in various p_T and x_F bins, is determined to be $6 \pm 1\%$.

4.2 *Efficiencies*

The combined π^0 acceptance and detection efficiency, shown in Fig. 3 as a function of p_T and of x_F, is about 40% for $p_T > 4.0$ GeV/c.

The losses due to γ conversions inside the target and in the Omega chambers (13%), geometry (10%), the trigger (6%) and the π^0 definition (13%), have been estimated by generating Monte Carlo events having high p_T $\pi^0 s$ with the same p_T and x_F distributions as in the data. A second Monte Carlo program, which was used also in this analysis, is based on the leading-order QCD hard scattering diagrams with the Lund model fragmentation [17]. These sets of Monte Carlo events were processed through a program which simulated the complete detector arrangement and, in addition, through the same chain of reconstruction programs as the data. The combined acceptances and efficiencies given by the two different simulations (ε_1 and ε_2) are statistically compatible. An estimate of systematic effects in the quantity $(\varepsilon_1 - \varepsilon_2)/\varepsilon_{\text{average}}$ gives a value compatible with zero with an upper limit of 0.15; these effects have been included in the systematic errors. The samples produced by the two different methods have been added together to cover the complete p_T range with statistical errors smaller than those of the data sample.

The loss of good events, due to the cuts applied to remove superposed and muon halo induced events (14%) and hadronic showers and electrons (3%), has been estimated from an analysis of $\pi^0 s$ in rejected events.

4.3 *Results*

The invariant cross section $Ed^3\sigma/dp^3$ for π^0 production averaged over each $p_T - x_F$ cell is given in Table 1 with both statistical and systematic errors. The p_T and x_F limits for each cell are indicated as well as their weighted averages. The p_T distribution for the central x_F region ($|x_F| < 0.15$) is shown in Fig. 4a. The two x_F regions $-0.45 < x_F < -0.15$ and $0.15 < x_F < 0.45$, compared in Fig. 4b, are consistent with each other within systematic errors. The x_F distributions for three separate p_T intervals are presented in Fig. 5.

The systematic errors in the cross section which vary with p_T and x_F as seen in Table 1 originate from:

a) the normalization uncertainty due to trigger losses and rejection of superposed events by TOF information amounting to about 6%;

b) the Monte Carlo statistical accuracy, the consistency of Monte Carlo corrections and the limited statistics of the π^0 data used to estimate the losses, contributing typically from 5 to 15%;

c) the energy scale uncertainty of 0.6% giving a normalization error increasing with p_T from 8 to 11%;

d) other systematic uncertainties, estimated by comparing the four quadrants in the 1984 and 1985

Table 1

Invariant cross section $Ed^3\sigma/dp^3$ (pbarn·GeV^{-2}) : $pp \to \pi^0 X$

cross sec.	±	stat. err.
	±	syst. err.

p_T =	4.0 – 4.25	4.25 – 4.5	4.5 – 4.75	4.75 – 5.0	5.0 – 5.5	5.5 – 6.0	6.0 – 6.5	6.5 – 7.0 GeV/c
$\bar{p}_T$ =	4.11	4.36	4.61	4.86	5.19	5.69	6.19	6.69 GeV/c
x_F = −0.45 / $\bar{x}_F$ = −0.393	196.7 ± 24.9 ± 39.	97.2 ± 12.8 ± 18.	36.3 ± 6.7 ± 6.5	16.1 ± 4.1 ± 3.1	5.9 ± 1.5 ± 1.2	0.94 ± 0.54 ± 0.23		
−0.35 / −0.295	303.9 ± 13.2 ± 56.	150.5 ± 8.5 ± 25.	71.5 ± 5.5 ± 12.	35.6 ± 3.6 ± 5.9	9.1 ± 1.2 ± 1.7	2.67 ± 0.65 ± 0.57	0.75 ± 0.18 ± 0.18	
−0.25 / −0.196	506.1 ± 13.0 ± 93.	227.9 ± 8.4 ± 38.	115.2 ± 5.9 ± 18.	44.0 ± 3.5 ± 7.2	21.6 ± 1.7 ± 4.1	2.44 ± 0.56 ± 0.49		
−0.15 / −0.098	609.2 ± 12.9 ± 113.	290.5 ± 8.7 ± 48.	135.6 ± 5.8 ± 21.	72.2 ± 4.3 ± 12.	20.4 ± 1.6 ± 3.8	5.03 ± 0.76 ± 1.00		
−0.05 / 0.000	675.0 ± 13.1 ± 124.	353.4 ± 9.5 ± 59.	153.0 ± 6.1 ± 24.	72.0 ± 4.2 ± 12.	27.5 ± 1.8 ± 5.2	5.43 ± 0.79 ± 1.1	1.06 ± 0.21 ± 0.37	0.14 ± 0.08 ± 0.04
0.05 / 0.098	671.3 ± 13.2 ± 123.	323.5 ± 8.9 ± 54.	142.7 ± 5.9 ± 23.	68.6 ± 4.0 ± 11.	24.4 ± 1.7 ± 4.6	6.04 ± 0.85 ± 1.2		
0.15 / 0.196	472.8 ± 11.9 ± 86.	217.7 ± 7.8 ± 36.	97.4 ± 5.1 ± 15.	45.9 ± 3.4 ± 7.4	13.6 ± 1.3 ± 2.6	2.48 ± 0.53 ± 0.50		
0.25 / 0.295	206.1 ± 8.3 ± 38.	111.3 ± 6.0 ± 19.	48.1 ± 3.9 ± 7.7	22.0 ± 2.5 ± 3.6	6.15 ± 0.94 ± 1.2	1.40 ± 0.44 ± 0.29	0.37 ± 0.13 ± 0.08	
0.35 / 0.393	111.1 ± 6.7 ± 20.	49.6 ± 4.3 ± 8.4	24.0 ± 3.1 ± 3.9	10.3 ± 2.0 ± 1.7	3.55 ± 0.82 ± 0.69	0.53 ± 0.30 ± 0.11		
0.45								

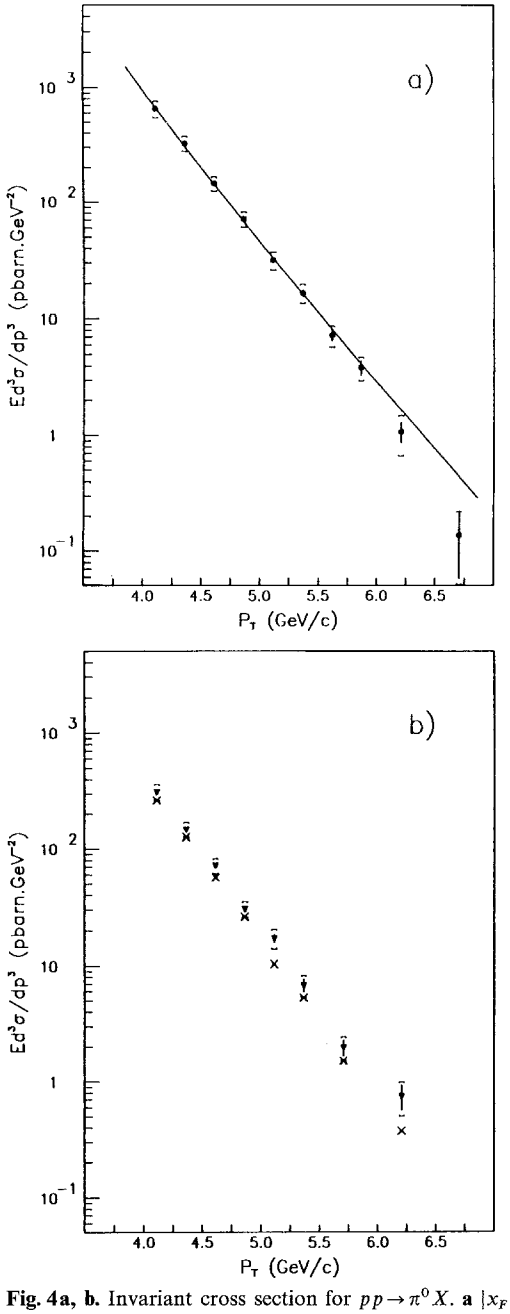

Fig. 4a, b. Invariant cross section for $pp \to \pi^0 X$. **a** $|x_F| < 0.15$. The curve shows the result of the phenomenological fit. **b** $-0.45 < x_F < -0.15$ (triangles) and $0.15 < x_F < 0.45$ (crosses). The error bars are statistical only. The errors obtained by combining statistical and systematic errors in quadrature are also indicated

data, and also comparing the data with Monte Carlo distributions, ranging from 8 to 16%.

4.4 Phenomenological fit and comparison with other experiments

A phenomenological expression,

$$E d^3\sigma/dp^3 = C(1-x_D)^m/(p_T/p_0)^{2n},$$

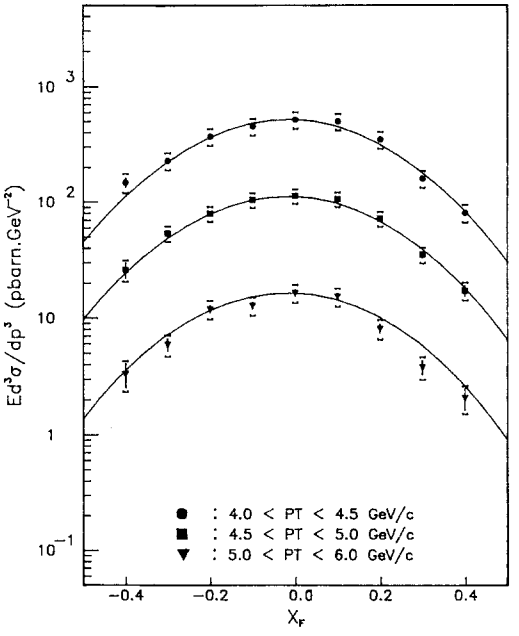

Fig. 5. Invariant cross section for $pp \to \pi^0 X$ as a function of x_F. The error bars are statistical only. The errors obtained by combining statistical and systematic errors in quadrature are also indicated. The curves show the results of the phenomenological fit

where

$$x_D = [x_T^2 + (x_F - x_0)^2]^{1/2},$$

$$x_T = 2p_T/\sqrt{s}, \quad p_0 = 1 \text{ GeV/c},$$

and where C, x_0, m and n are free parameters, has been fitted to the data using a maximum likelihood method [12] in a two-dimensional $x_F - p_T$ grid with bin sizes 0.025 and 0.25 GeV/c, respectively. The results of the fit are given in Table 2 and superimposed on the data in Figs. 4a and 5. The correlation matrices in Table 2 show that the fit parameters are strongly correlated; the factor C, in particular, is very dependent on the other parameters, especially on n, and should not be taken as a cross section measurement by itself. The fit took into account only the statistical errors. In order to estimate the systematic effects on the fit parameters, separate fits have been performed on the 1984 and 1985 data. Systematic discrepancies observed at the edges of the x_F distributions affect mainly the parameters m and n which can change from 6 to 7% and 4 to 6%, respectively, relative to the values quoted in the table. The separate fits to the 1984 and 1985 data yield cross sections which are compatible with the values quoted in Table 1 within systematic errors.

In proton-proton interactions, the symmetry of the partons in the beam and target particles implies that $x_0 = 0$. The non-zero value of this parameter is therefore an indication of systematic errors.

Table 2. Parameters of the phenomenological fit

$pp \to \pi^0 X$		C(mb/GeV^2)	m	n	x_0
Value ± stat. error		16.4 ± 2.5	5.26 ± 0.09	5.16 ± 0.06	−0.018 ± 0.002
Correlation	C		−0.310	0.959	−0.173
Coefficients	x_0		0.419	−0.267	
	n		−0.565		
$pp \to \gamma X$		$C(\mu$b/GeV^2)	m	n	x_0
Value ± stat. error		7.3 ± 6.1	3.76 ± 0.48	3.73 ± 0.25	−0.054 ± 0.017
Correlation	C		0.591	0.803	−0.232
Coefficients	x_0		−0.481	−0.420	
	n		0.955		

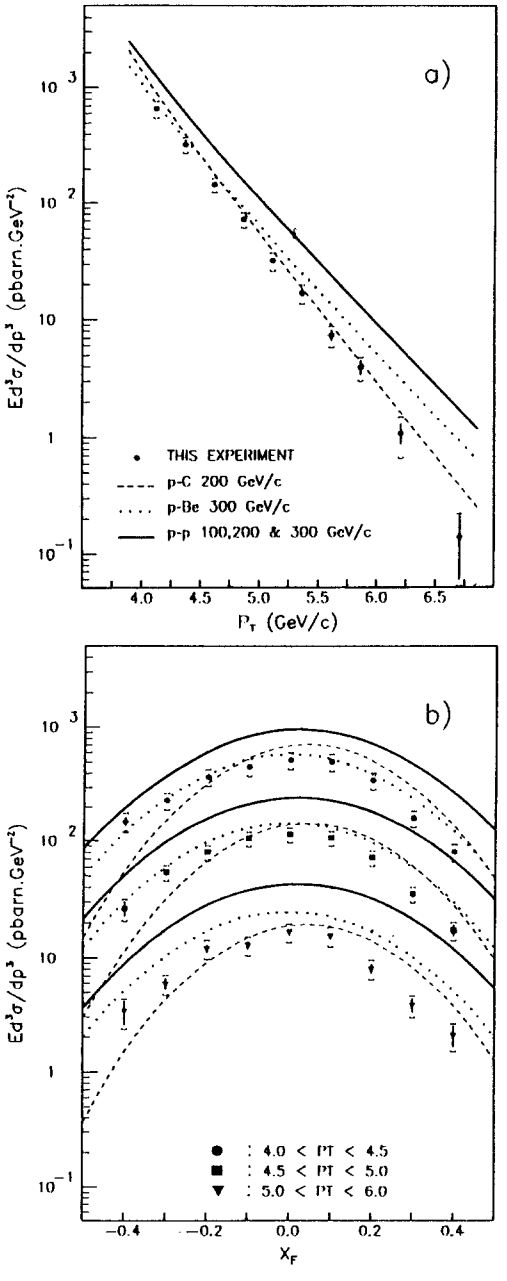

Fig. 6a, b. Comparison with the fits given by other experiments, extrapolated into the kinematical range of the present experiment: pC at 200 GeV/c [19], pBe at 300 GeV/c [20] and pp at 100, 200 and 300 GeV/c [18]. **a** $|x_F| < 0.15$. **b** $4.0 < p_T < 4.5$ GeV/c, $4.5 < p_T < 5.0$ GeV/c and $5.0 < p_T < 6.0$ GeV/c

Table 3. Kinematical range of experiments

Reference	Target	Beam momentum (GeV/c)	Kinematical range
Present Data (WA 70)	Hydrogen	280	$4.0 < p_T < 6.5$ GeV/c $-0.45 < x_F < 0.45$
C. De Marzo et al. [10]	Hydrogen	300	$1.25 < p_T < 7.0$ GeV/c $-0.65 < y^* < 0.52$
G. Donaldson et al. [18]	Hydrogen	100, 200, 300	$0.4 < p_T < 4.5$ GeV/c $-0.2 < x_F < 0.8$
J. Badier et al. [19]	Carbon	200	$2.9 < p_T < 6.0$ GeV/c $0.4 < y^* < 1.2$
R. Baltrusaitis et al. [20]	Beryllium	300	$1.2 < p_T < 6.0$ GeV/c $-0.8 < x_F < 0.0$

Similar fits available from other experiments [18, 20] are superimposed on the present data in Fig. 6. The conditions in which the data for these fits have been obtained are summarized in Table 3. The fit by Donaldson et al. [18] (full line), obtained from the data in a lower p_T range than that of the present data, shows deviations of up to a factor 4 for $p_T > 4.0$ GeV/c. The results of Badier et al. [19] (dashed line) show a good agreement with the present data in p_T except for a shift in x_F. The fit by Baltrusaitis et al. [20] (dotted line) shows a difference in p_T but agrees in the x_F distribution (the central value was fixed at zero in their analysis).

Finally, the data of De Marzo et al. [10], on pp interactions at 300 GeV/c (Table 3), have been compared with our fit; their cross section, measured as

a function of p_T only, agrees with the prediction of our fit within 20% for $p_T > 2$ GeV/c.

5 Prompt photon analysis

5.1 Data selection

Prompt photon candidates are chosen from the events selected as described in Section 3, by demanding that the trigger shower does not form an effective mass with any other shower in any hypothesis in the $\pi^0(\eta)$ mass range from 70 to 200 MeV (450 to 650 MeV) with a decay asymmetry smaller than 0.99 (0.90). The $\gamma\gamma$ effective mass cuts in the π^0 and η regions are shown in Fig. 7. In addition the shower must be inside a fiducial region extending to 5 cm from the edges of each quadrant and have a transverse width (σ), integrated over the three segments, smaller than 2 cm.

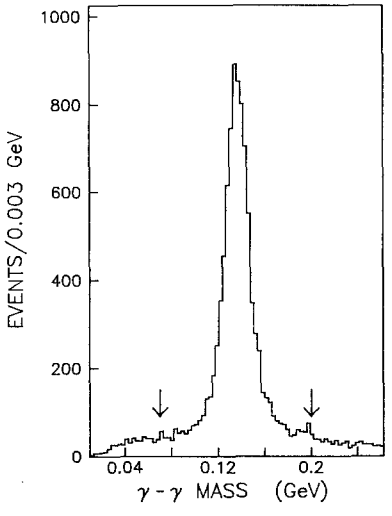

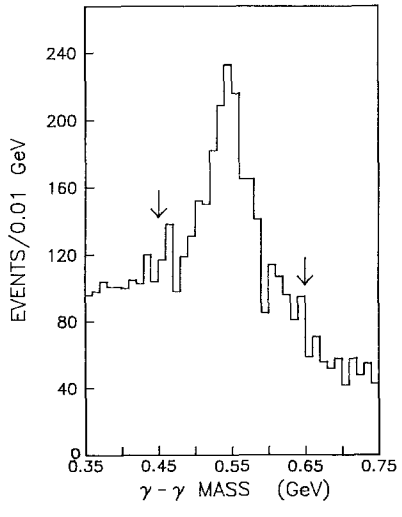

Fig. 7a, b. The $\gamma\gamma$ effective mass spectrum, obtained by taking into account all possible hypotheses of shower configurations and plotting only those nearest to the π^0 or η mass. **a** π^0 mass region. **b** η mass region. The arrows define the π^0 and η mass intervals

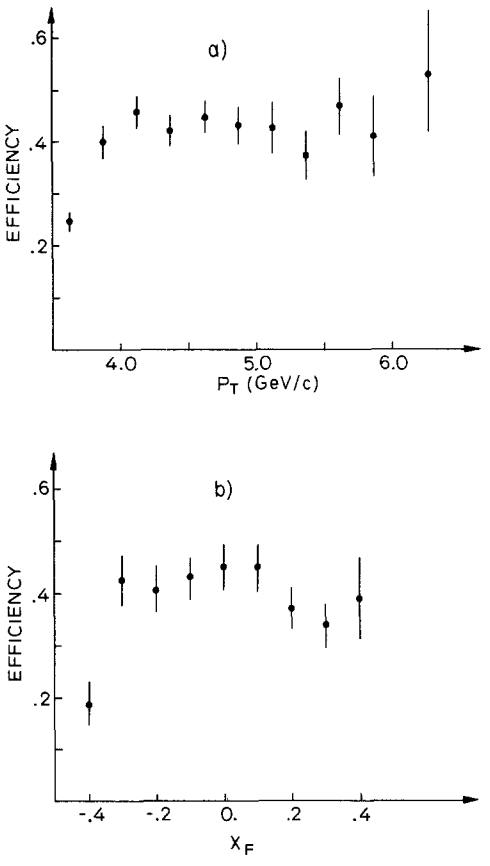

Fig. 8a, b. The combined prompt photon acceptance and analysis efficiency, obtained by Monte Carlo and by analysis of rejected events. **a** $|x_F| < 0.15$. Only the region $p_T > 4.0$ GeV/c has been used. **b** $4.5 < p_T < 5.0$ GeV/c. Only the region $x_F > -0.35$ has been used. The error bars show the Monte Carlo statistical errors and systematic uncertainties as well as the estimated systematic effects from rejected events. The different errors are added in quadrature

5.2 Efficiencies

The Monte Carlo events, generated with leading order QCD hard scattering diagrams with Lund model fragmentation [17], have been used to estimate losses due to various sources. These are photon conversion (6%), geometrical acceptance (8%), trigger effects (3%), rejection of faked $\pi^0 s$ (8%) and ηs (6%), and fiducial region cuts (6%). The losses due to cuts to remove superposed events, muon halo events, hadronic showers and electrons, have been assumed to be the same as those obtained for the π^0 analysis.

The overall prompt photon efficiency is around 45% for $p_T > 4.0$ GeV/c (Fig. 8).

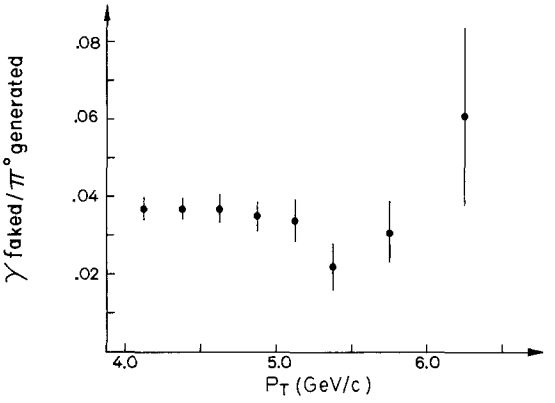

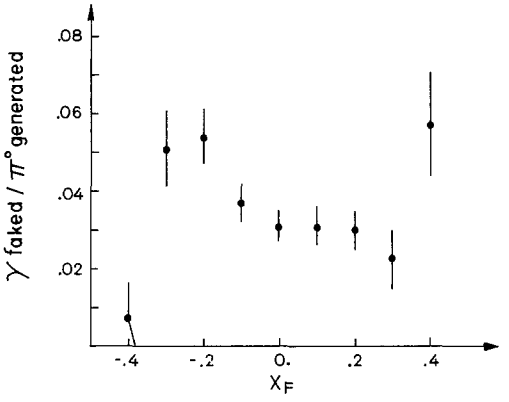

Fig. 9a, b. Ratio of faked γ background to π^0s generated by Monte Carlo. **a** $|x_F|<0.15$. **b** $4.5<p_T<5.0$ GeV/c. Only the region $x_F>-0.35$ has been used

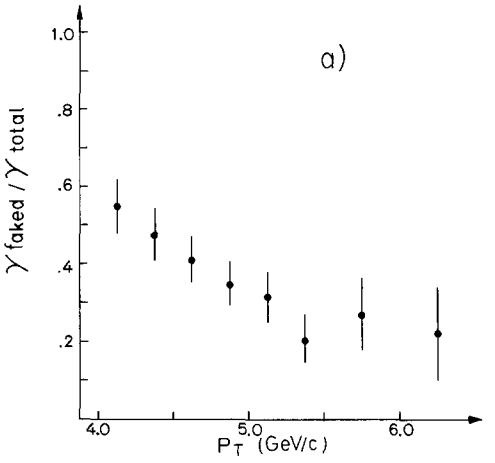

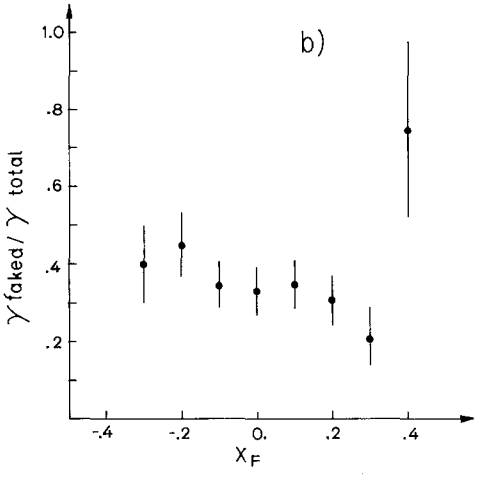

Fig. 10a, b. Faked γ background normalized to prompt photon candidates in the data. **a** $|x_F|<0.15$. **b** $4.5<p_T<5.0$ GeV/c

Table 4

Invariant cross section $Ed^3\sigma/dp^3$ (pbarn·GeV^{-2}) : $p\,p \to \gamma\,X$

cross sec. ± stat. err. ± syst. err.

p_T =	4.0	4.25	4.5	5.0	5.5	6.0	6.5 GeV/c
$\bar{p}_T$ =	4.11	4.36	4.70	5.20	5.70	6.20	GeV/c
x_F = −0.35	22.6 ± 4.0 ± 6.8	9.5 ± 3.2 ± 4.5	5.9 ± 1.2 ± 1.6	2.82 ± 0.78 ± 0.77			
$\bar{x}_F$ = −0.295 −0.25	31.4 ± 4.4 ± 8.6	22.9 ± 2.9 ± 5.0	8.4 ± 1.5 ± 2.0	1.97 ± 0.65 ± 0.57	0.66 ± 0.37 ± 0.25	0.27 ± 0.15 ± 0.20	
−0.197 −0.15	29.6 ± 4.0 ± 8.2	24.9 ± 3.3 ± 5.7	10.2 ± 1.4 ± 2.1	2.87 ± 0.70 ± 0.68	0.72 ± 0.34 ± 0.24		
−0.098 −0.05	32.6 ± 3.9 ± 8.5	24.0 ± 3.3 ± 5.7	10.5 ± 1.4 ± 2.1	3.92 ± 0.87 ± 0.94	0.68 ± 0.32 ± 0.22	0.22 ± 0.10 ± 0.11	
0.00 0.05	19.9 ± 3.7 ± 7.2	19.4 ± 4.3 ± 6.8	9.4 ± 1.6 ± 2.2	2.35 ± 0.66 ± 0.61	0.62 ± 0.33 ± 0.23		
0.098 0.15	19.9 ± 4.0 ± 7.2	17.5 ± 2.8 ± 4.3	8.8 ± 1.4 ± 1.9	2.12 ± 0.58 ± 0.53	0.59 ± 0.34 ± 0.24		
0.197 0.25	12.0 ± 2.7 ± 3.6	6.5 ± 2.1 ± 2.7	5.7 ± 1.2 ± 1.4	1.69 ± 0.57 ± 0.47	0.26 ± 0.22 ± 0.11	0.03 ± 0.03 ± 0.02	
0.295 0.35	11.6 ± 3.5 ± 4.7	4.5 ± 2.0 ± 2.1	0.85 ± 0.69 ± 0.58	0.95 ± 0.70 ± 0.50			
0.393 0.45							

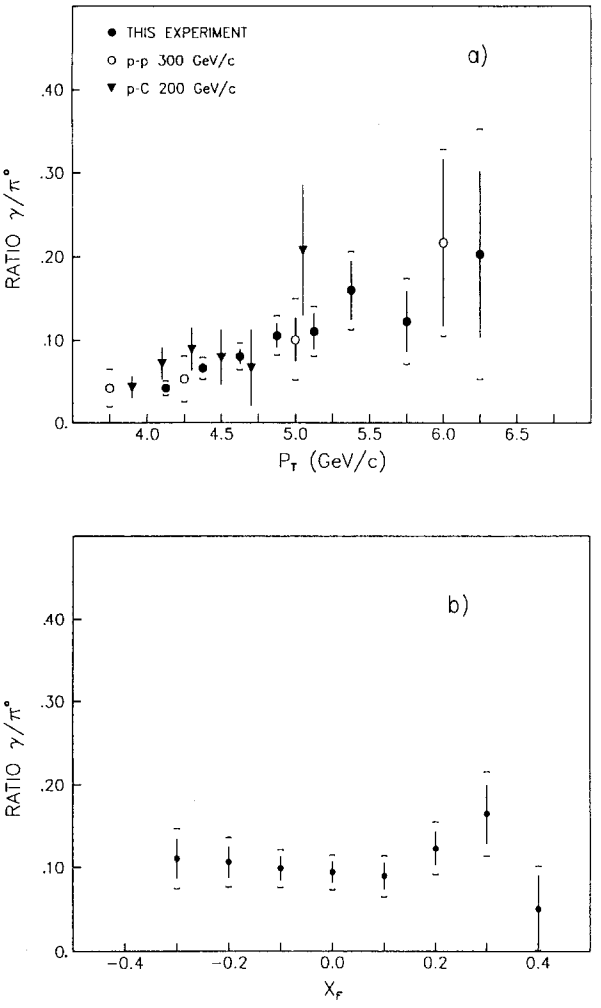

Fig. 11a, b. Ratio of production cross sections $\sigma(pp \to \gamma X)/\sigma(pp \to \pi^0 X)$. **a** $|x_F|<0.15$. Also plotted are other fixed target experiments: $p-C$ at 200 GeV/c [9] and $p-p$ at 300 GeV/c [10]. **b** $4.5 < p_T < 5.0$ GeV/c

5.3 Background

The background in the prompt photon signal due to unreconstructed $\pi^0 s$ (60%), ηs (31%), $\eta' s$ and decay of hadrons (9%) has been evaluated by the Lund Monte Carlo. Fake prompt photons can arise from several mechanisms:

a) The $\gamma\gamma$ decay is asymmetric and one γ escapes detection by being outside the geometrical acceptance or below the energy threshold. This background is dominant at low p_T and negative x_F.

b) The two photons from a π^0 are not resolved by pattern recognition. This background amounts to 2.5% integrated over the kinematical region covered by the data, but reaches 40% at $x_F=0.4$.

c) One γ converts in the target or the MWPCs, or it is not reconstructed by pattern recognition. Figure 9 shows the fraction of faked photons normalized to the number of generated $\pi^0 s$. The background in the prompt photon sample has been obtained by multiplying this ratio with the measured π^0 cross section. The ratio γ (faked)/γ (total) as a function of p_T and of x_F is given in Fig. 10. The contamination in the raw prompt photon sample due to unidentified hadronic showers, electrons and muon halo events, is negligible. The uncertainty in this estimate is 5% for hadrons and electrons while for muon halo events it varies from 0.5 to 10% for p_T in range of 4.0 to 6.5 GeV/c. Below $x_F=-0.35$, the γ background cannot be reliably estimated due to low and and rapidly varying acceptance in this region.

5.4 Results

The inclusive invariant cross section $Ed^3\sigma/dp^3$ averaged over each p_T-x_F cell is presented in Table 4 for $p_T>4$ GeV/c and $-0.35<x_F<0.45$. The ratio γ/π^0 is shown in Fig. 11 as p_T and x_F projections. This ratio increases with p_T and is weakly dependent on x_F. It is compared in Fig. 11a with other fixed target experiments [9, 10] with comparable kinematical ranges. The p_T and x_F distributions of the cross section are shown in Figs. 12 and 13.

Systematic errors for the γ cross section, in addition to the contributions discussed in Sec. 4.3, arise from background subtraction. The Monte Carlo statistical uncertainties of 12 to 40% for the background lead to an error between 10 and 25% in the γ cross section. The uncertainty in the calculation of the hadron shower contamination also produces an error between 7 and 10% in the cross section. The corresponding figure for muon halo events is 1% for $p_T=4$ GeV/c rising to 12% at 6.5 GeV/c. The different contributions, added quadratically, are given as total systematic errors in Table 4.

The prompt photon cross sections may be represented by the same phenomenological function as that for the π^0 cross section. A least-squares fit has been performed using only the statistical errors. The fitted parameters are given in Table 2. It is to be noted that the value of n, characteristic of the p_T dependence, is smaller by one unit than that for π^0 production.

The cross sections for production of $\pi^0 s$ and prompt photons by incident protons are compared in Fig. 14 with those by incident $\pi^+ s$ in the same positive beam [12, 11] in the central x_F region ($|x_F|<0.15$). The ratio $\sigma(\pi^+ p)/\sigma(pp)$ is greater than one for $p_T>4.0$ GeV/c and increases with p_T, as expected from the parton model.

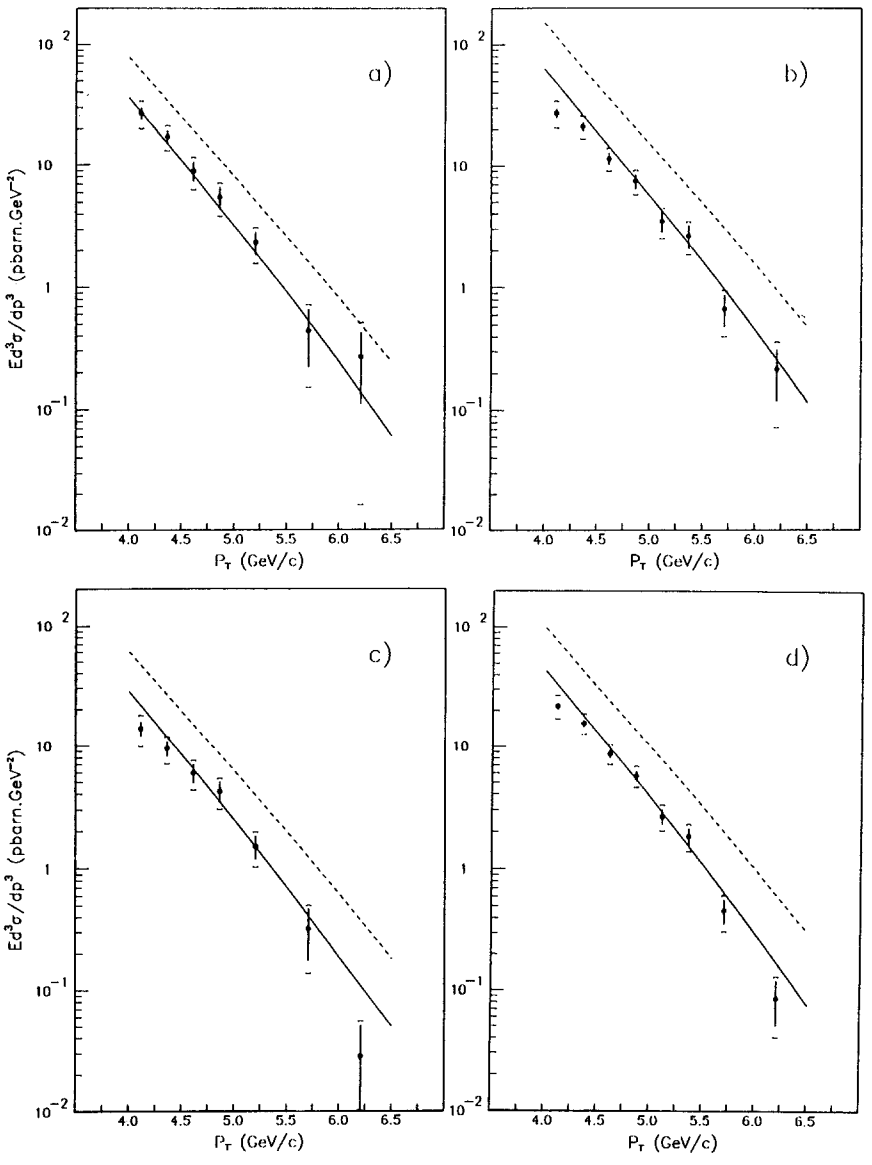

Fig. 12a–d. Invariant cross section for $pp \to \gamma X$.
a $-0.35 < x_F < -0.15$.
b $-0.15 < y_F < 0.15$.
c $0.15 < x_F < 0.45$.
d $-0.35 < x_F < 0.45$. The error bars are statistical only. The errors obtained by combining statistical and systematic errors in quadrature are also indicated. The curves shown correspond to the predictions of second order QCD calculations [2] using optimized scales with Duke and Owens structure functions [23], set 1 (full) and set 2 (dashed), respectively

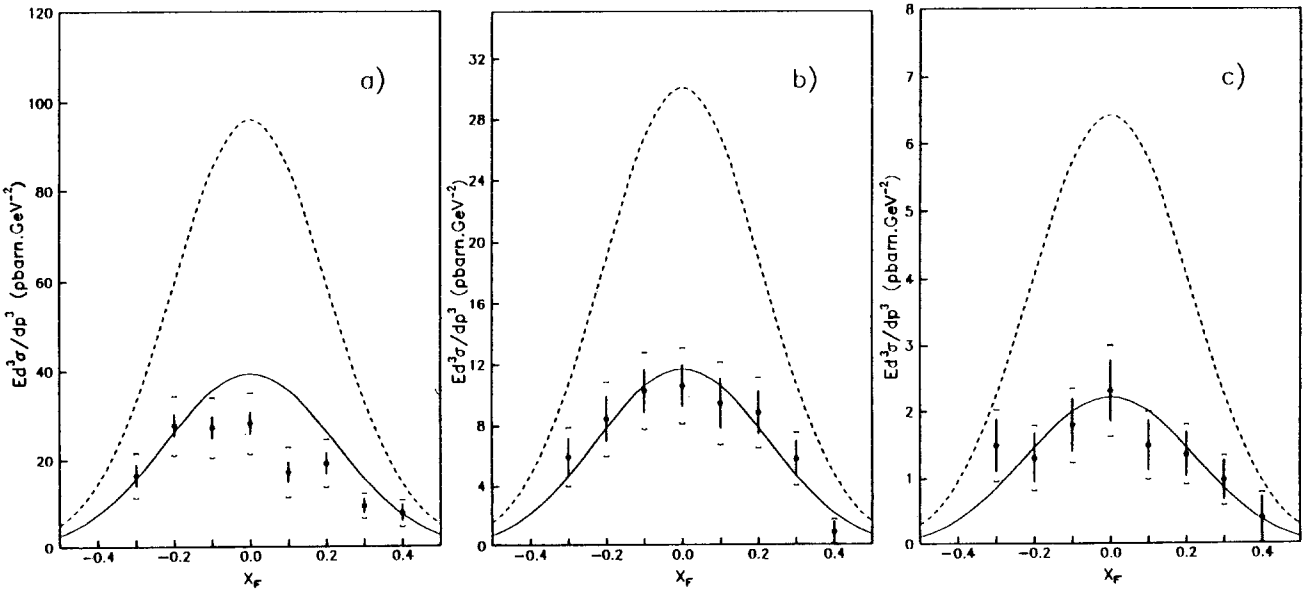

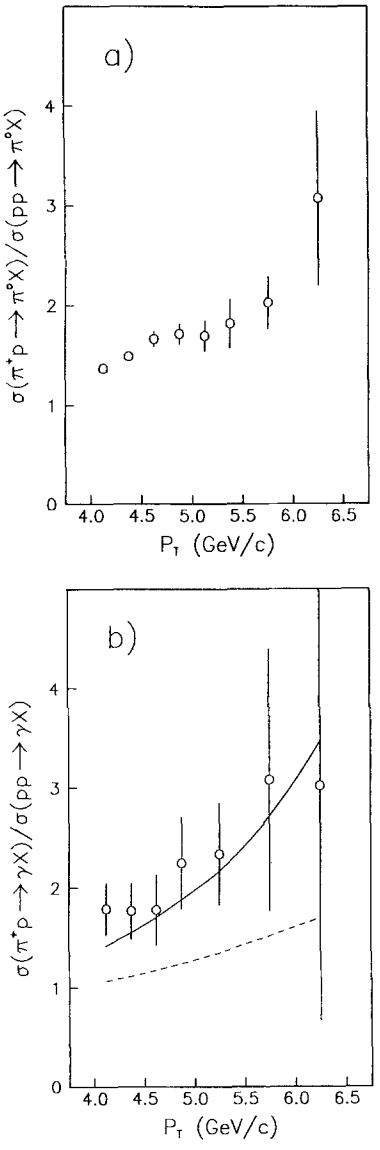

Fig. 14a, b. Ratio $\sigma(\pi^+ p)/\sigma(pp)$ as a function of p_T for $|x_F|<0.15$. The errors are statistical only; the systematic errors are estimated to be smaller than the statistical errors. **a** π^0 production, **b** prompt photon production. The curves correspond to the second order QCD calculation [2] with the Duke and Owens structure functions [23], set 1 (full) and set 2 (dashed), respectively

6 Comparison with QCD predictions

The prompt photon cross section is compared in Figs. 12 and 13 with a complete next-to-leading order QCD calculation [2]. The optimised scales [21, 22] used in the program for factorization and renormalization have been calculated for each $x_F - p_T$ cell and for the two sets of structure functions of Duke and Owens [23]. These structure functions have been obtained by fitting data from deep inelastic scattering, the Drell-Yan process and J/ψ production. Quark and gluon distributions are parametrized to leading-log accuracy in the Q^2 dependence. The gluon distribution has a shape strongly correlated to the QCD scale parameter Λ. The fits, at an input value $Q_0^2 = 4.0$ (GeV/c)^2, are

set 1: $\Lambda = 200$ MeV/c and soft gluon,
$xG(x) \approx (1+9x)(1-x)^6$,

set 2: $\Lambda = 400$ MeV/c and hard gluon,
$xG(x) \approx (1+9x)(1-x)^4$.

Table 5. Comparison with QCD theory

	Set 1 x^2/d.o.f.	Set 2 x^2/d.o.f.
$-0.35 < x_F < -0.15$	1.49/7	83.8/7
$-0.15 < x_F < 0.15$	11.43/8	525.9/8
$0.15 < x_F < 0.45$	8.3/7	255.1/7
$4.0 < p_T < 4.5$ GeV/c	19.4/8	436.6/8
$4.5 < p_T < 5.0$ GeV/c	3.5/8	206.5/8
$5.0 < p_T < 6.0$ GeV/c	2.65/8	225.9/8
$4.0 < p_T < 6.0$ GeV/c and $-0.35 < x_F < 0.45$	35.2/38	1070.0/38

Figures 12 and 13 show that set 1 (full line) is compatible with our data, whilst set 2 (dashed line) is excluded in all p_T and x_F intervals. The ratio $\sigma(\pi^+ p \to \gamma X)/\sigma(pp \to \gamma X)$, which is not affected by systematic errors in the absolute normalization, also agrees with the parameters of set 1 and excludes set 2, as shown in Fig. 14b. Table 5 gives a quantitative comparison of the present data with the theoretical predictions taking into account statistical and systematic errors.

The ratio K=(data/prediction) for set 1 is shown in Fig. 15 as a function of p_T; deviations from $K=1$ are within the systematic errors in the p_T range 4.25 to 6.0 GeV/c but become significant outside this p_T range.

7 Conclusions

The present experiment has determined the inclusive γ and π^0 cross sections with 280 GeV/c protons incident on a hydrogen target, in the transverse momentum and Feynman x_F ranges, $4.0 < p_T < 7.0$ GeV/c and $|x_F| < 0.45$ for π^0 production, and $4.0 < p_T < 6.5$ GeV/c and $-0.35 < x_F < 0.45$ for γ production, respectively.

Fig. 13a–c. Invariant cross sections for $pp \to \gamma X$ and QCD predictions. **a** $4.0 < p_T < 4.5$ GeV/c. **b** $4.5 < p_T < 5.0$ GeV/c. **c** $5.0 < p_T < 6.0$ GeV/c. The same comments apply as in the previous figure

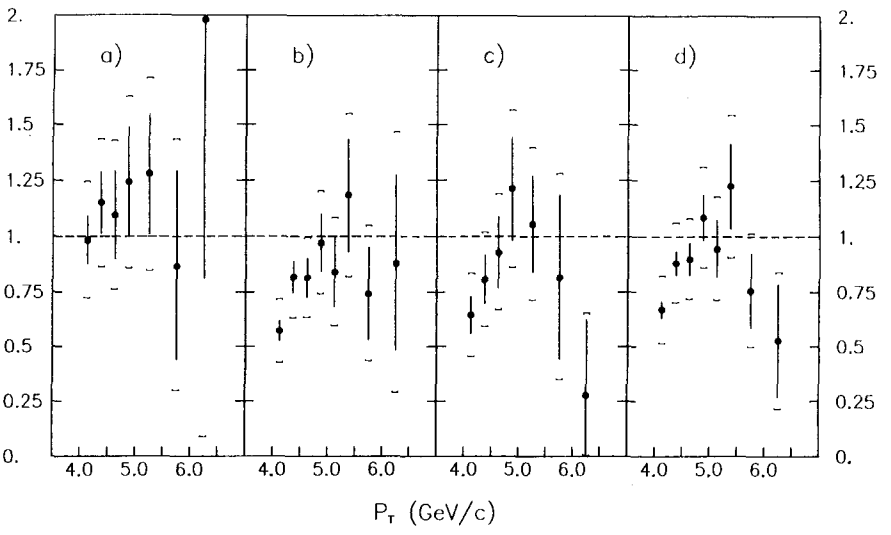

Fig. 15a–d. Ratio K=(data/QCD prediction [2]) for the Duke and Owens structure function set 1 [23]. **a** $-0.35<x_F<-0.15$, **b** $-0.15<x_F<0.15$, **c** $0.15<x_F<0.45$, **d** $-0.35<x_F<0.45$

The cross sections have been fitted to the following phenomenological expression:

$$E d^3\sigma/dp^3 = C(1-x_D)^m/(p_T/p_0)^{2n},$$
$$x_D = [x_T^2+(x_F-x_0)^2]^{1/2}.$$

The results show a steeper p_T dependence for π^0 than for prompt photon production.

The π^0 data of the present experiment are in agreement with the extrapolated fits from other experiments within 10 to 30% at $x_F \approx 0$ and low p_T, but can differ by a factor of four in the regions of low cross section for $p_T > 6.0$ GeV/c and at the edges of the x_F distribution.

A quantitative comparison of the γ cross section with QCD second order calculations [2] shows good agreement within systematic errors for $p_T > 4.25$ GeV/c, if the optimized scales [21, 22] and a soft gluon structure function with $\Lambda = 200$ MeV/c (set 1 of Duke and Owens [23]) are used. The data are incompatible with the hard gluon structure function with $\Lambda = 400$ MeV/c (set 2 of Duke and Owens [23]).

Acknowledgements. It is a pleasure to thank the members of the Omega support group, especially W. Beusch and F. Bourgeois as well as the EA and DD/OC support groups, for their invaluable assistance throughout the experiment. We have benefitted from the computing facilities provided by CERN, CILEA, RAL and University of Geneva. In addition, we acknowledge financial support from CERN, INFN, the United Kingdom SERC and the Swiss National Fund.

We thank P. Aurenche, R. Baier, A. Douiri, M. Fontannaz and D. Schiff for allowing us to use their computer program on the next-to-leading order QCD calculation with scale optimization. Finally, we are grateful to P. Aurenche and G. Ingelman for helpful discussions, and to S. Chung for his comments during the preparation of this paper.

References

1. J.F. Owens: Rev. Mod. Phys. 59 (1987) 465
2. P. Aurenche et al.: Phys. Lett. 140B (1984) 87; P. Aurenche, R. Baier, M. Fontannaz, D. Schiff: Orsay preprint LPTHE 87/30 (1987)
3. P. Darriulat et al.: Nucl. Phys. B110 (1976) 365
4. E. Amaldi et al.: Phys. Lett. 77B (1978) 240
5. M. Diakonou et al.: Phys. Lett. 87B (1979) 292
6. A.L.S. Angelis et al.: Phys. Lett. 94B (1980) 106
7. T. Åkesson et al.: Phys. Lett. 123B (1983) 367
8. For complete list of experiments before 1984, see T. Ferbel, W.R. Molzon: Rev. Mod. Phys. 56 (1984) 181
9. J. Badier et al.: Z. Phys. C31 (1986) 341
10. C. De Marzo et al.: Phys. Rev. D36 (1987) 8; ibid D36 (1987) 16
11. M. Bonesini et al.: Z. Phys. C – Particles and Fields 37 (1988) 535
12. M. Bonesini et al.: Z. Phys. C–Particles and Fields 37 (1987) 39
13. C. Bovet et al., CERN yellow report 82-13
14. M. Bonesini et al.: A lead-liquid scintillator electromagnetic calorimeter for direct photon pyhsics to be published in Nucl. Instum. Methods
15. M. Bonesini et al.: A 1152 channel timing system for an electromagnetic calorimeter readout to be published in Nucl. Instum. Methods
16. P. Béné et al.: High p_T trigger electronics for a large orthogonal readout electromagnetic calorimeter preprint CERN-EP/87–200, submitted to Nucl. Instrum. Methods
17. H.U. Bengtsson, G. Ingelman, T. Sjöstrand: The Lund Monte Carlo for high p_T scattering. PYTHIA version 4.1, update of H.U. Bengtsson, G. Ingelman: Comp. Phys. Commun. 34 (1985) 251; T. Sjöstrand. Jet fragmentation JETSET version 6.2, Comp. Phys. Commun. 39 (1986) 347
18. G. Donaldson et al.: Phys. Lett. 73B (1983) 375
19. J. Badier et al.: Z. Phys. C – Particles and Fields 30 (1986) 45
20. R.M. Baltrusaitis et al.: Phys. Rev. Lett. 44 (1980) 122
21. P.M. Stevenson: Phys. Rev. D23 (1981) 2916; H.D. Politzer: Nucl. Phys. B194 (1982) 493; P. Stevenson, H. Politzer: Nucl. Phys. B277 (1986) 758
22. P. Aurenche, R. Baier, M. Fontannaz, D. Schiff: Nucl. Phys. B286 (1987) 509
23. D.W. Duke, J.F. Owens: Phys. Rev. D30 (1984) 49